Doctoral dissertation

Prepared in the Institute of Physics of the Jagiellonian University

Submitted to the Faculty of Physics, Astronomy and Applied Computer Science of the Jagiellonian University

Investigations of mechanisms of particle production in proton-induced nuclear spallation

Udai Singh

Supervised by:
prof. dr hab. Krzysztof Pysz

Co-supervised by:
dr. Sushil Sharma

Cracow 2021

Contents

Abstract

The aim of the present work was to assess the model capabilities in describing the proton induced spallation reactions. To understand the reaction mechanism, different sets of observables must be investigated, inclusive as well as exclusive. Based on these criteria, the eforts were done to survey the scientific literature for the selection of representative data sets which its the need. The selected data were rich in terms of production of various ejectiles: neutrons, light charged particles (LCP: p, d, t, 3He, 4He), intermediate mass fragments, i.e., the particles with atomic mass number (LCP, IMF , fissionfragments), and target-like heavy residua. Several atomic nuclei from Al up to Pb were selected as representative for all the targets. The proton beam covered the broad range of energies from 180 MeV to 3000 MeV. The spallation reaction was treated as a two stage process. In the first stage, the incident proton initiates the cascade of binary collisions with target nucleons leaving behind an excited remnant. The second stage consists in the decay of this excited remnant nucleus. The selection of best models to describe each of these two stages was done on the basis of previous benchmark eforts where INCL4.5 model was found to be the best to describe the first stage of the reaction. Therefore the newest version of this model - INCL4.6 was used in the present study. Four theoretical models different in approach to the reaction mechanism were chosen to realize the description of the second stage: ABLA07, GEMINI++, SMM, GEM2. Qualitative as well as quantitative comparisons of model calculations with experimental data were undertaken. To judge the quality of models the agreement in magnitude of different observables with model predictions as well as reproduction of the shape of the mass, angle and energy distributions of the cross sections were taken into account. Various deviation factors were used for providing ranking and validation of the spallation models. The statistical properties of the test factors

Dedication

To mum and dad

Declaration

I declare that..

Acknowledgements

I want to thank...

Chapter 1

Introduction

1.1 Spallation reaction

The spallation reaction is a nuclear reaction in which a target nucleus struck by an incident particle of energy greater than around 50 MeV ejects numerous lighter particles and becomes a product nucleus correspondingly lighter than the original nucleus.
Nuclear Physics Academic press definition of spallation reaction[ref]:
"A type of nuclear reaction in which the high-energy of incident particles causes the nucleus to eject more than three particle, thus changing both its mass number and its atomic number."

1.1.1 Why spallation reaction?

According to the above definition, the spallation reactions lead to a significant modification of the initial nucleus thus various mechanisms of the nuclear processes may contribute. Understanding of these processes is interesting by itself but, moreover, it is necessary for numerous scientific and technological applications.The spallation reaction plays very important role in a wide domain of applications which are like neutron sources for material science studies [1], conversion of nuclear waste into non radioactive substances or short life products[2] as well as production of short life rare isotopes for medical science studies [3] and scientific purposes, [4],simulation of detector set-ups in nuclear and particle physics experiments, and radiation protection near accelerators or in space. The simulation tools developed for these

domains apply nuclear model codes to compute the production yields and characteristics of all the particles and nuclei generated in these reactions.

The recent activities in production of Rare Isotope Beams and Spallation Sources led to revival of interest in reliable and predictive simulation of collisions of hadron-nucleus and nucleus-nucleus in the energy range of few hundred MeV to few GeV per particle, to be embedded in transport codes (e.g. MCNPX, GEANT). Owing to the complexity of the quantum-mechanical many-body problems, the processes are often solved approximately.

1.1.2 Need for theoretical models

Such a broad range of applications of the spallation reactions demands the knowledge of the cross sections for production of various nuclides, frequently in interaction of protons with unstable and short living atomic nuclei. In this case it is difficult, time consuming and/or very expensive to obtain experimentally a desirable information. Therefore an existence of a reliable theory of the mechanisms contributing to the spallation reactions is necessary. Unfortunately, the present day status of the nuclear reaction theory does not allow to solve exactly such a multi body nuclear problem. Thus in practice various simplified models of the spallation reactions are proposed.Most of these models assume a two-step mechanism few of them also assume three step mechanism of nuclear reaction.

1.1.3 Types of models

There are various models available for proton induced spallation reaction and also works for other possible projectiles and reactions for example INCL++ [5], GiBUU[ref], UrQMD[ref], JAM[ref], Bertini[ref], CEM[ref], ISABEL[ref], etc . Depending on the projectile energy, target mass, and interested ejectiles the best models can be chosen. Most of them assume a two-step mechanism of the reactions few models are also assume pre-equilibrium process also.

- The first stage of the reaction consists of an intranuclear cascade (INC) of nucleon-nucleon and nucleon-pion collisions which leads to an abundant emission of nucleons and pions leaving the excited residuum of the target nucleus in a thermodynamical equilibrium.
- In the second stage of the process a de-excitation of the residual excited nucleus appears by emission of nucleons and complex nuclei due to the

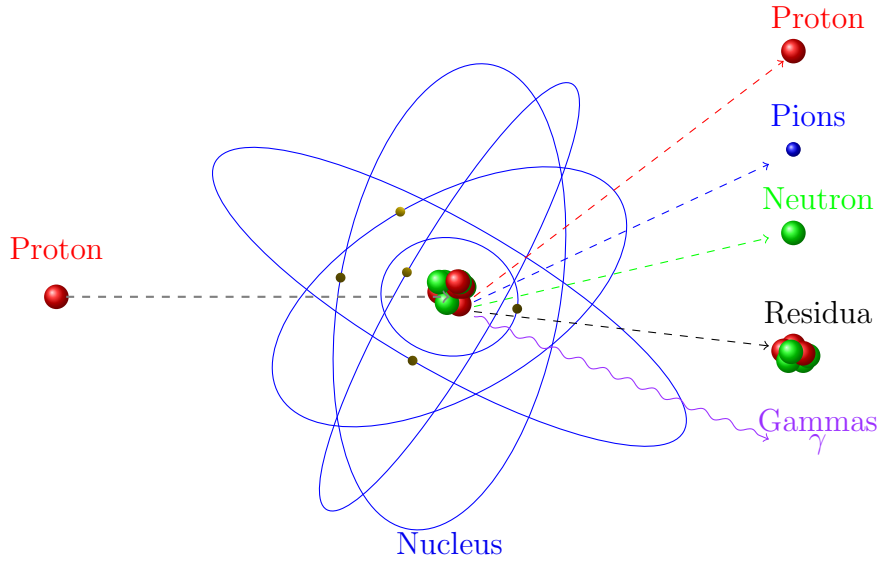

Figure 1.1: Possible particle production in the first stage of the spallation reaction

nuclear evaporation, fission and/or fragmentation.

An advanced representative of such models of the first stage of the spallation reactions is the Liège INC model which in its INCL4.2 version [6] is able to successfully describe the total cross sections as well as the energy spectra and angular distributions of neutrons, protons and pions in the broad range of the proton or deuteron projectile energies (from 50 MeV to 5 GeV). Furthermore, when coupled with the specific model of the de-excitation of heavy residual nuclei, *i.e.*, ABLA [7] it is able to reproduce experimental yields of heavy, target - like reaction remnants. However, this model - similarly as all other spallation models - meets a problem of the explanation and quantitative description of the non-equilibrium emission of complex light charged particles (LCP), *i.e.*, d, t, ^{3}He and ^{4}He as well as the intermediate mass fragments (IMF), *i.e.*, particles heavier than ^{4}He but lighter than products of the fission.

1.2 Questions to be answered

After many year of research in this field still many questions are unanswered the few of them are:

- Which of the models of the second stage of the reaction is the best in reproduction of selected observables (total and isotopic cross sections) - with the assumption that INCL is the best, realistic model of the first stage. On the basis of the literature data.
- The extraction of new experimental DIFFERENTIAL cross sections of the protons, pions and deuterons with the aim to check whether INCL is able to reproduce well high energy tail of the spectra (what is necessary to claim that INCL is a good model)
- To check whether other popular models of the 1st stage are equally good as the INCL model in description of these particles (NOTE: protons are the most abundant charged particles and heavier particles probably may be treated as not important in decision whether the main mechanism is reproduced)
- To check how the properties of the residual nuclei after the 1st stage depend on the applied model

1.3 Organization of thesis

The general objective of this work was to study the mechanisms of pions, proton and nuclear composite particles production in proton-nucleus collisions. The studies were performed partially experimental – utilizing the data of the HADES collaboration and analysing that data to extract the cross-section for p,d,t, and pions, and to some extent theoretical, in the sense that the validation of the existing theoretical models is performed. Two, qualitatively different investigations were undertaken in the present thesis:

- The theoretical analysis of the published in the literature data, which contain total isotopic cross sections for production of nuclei from Li to Ba in p+136Xe reaction at Ep=1 GeV and differential as well as total cross sections available for p+Ag collisions at Ep=0.48 GeV with production of isotopes of Li, Be, ... Mg nuclei. Results of this analysis were partially published [8] and [9].

- The experimental determination of the differential cross section $d\sigma/d\Omega dE$ for emission of Hydrogen isotopes as well as pion π^+ and π^- from collisions of protons with Nb nuclei at Ep=3.5 GeV (HADES collaboration) and theoretical description of the obtained data.

Chapter 2

Contemporary theoretical models used for description and interpretation of the experimental data

In this chapter various model describing the mechanism of proton induced spallation reaction will be discussed.As it is described in the Introduction that the spallation reaction is a two step process fist fast stage which occures in few fm/c and second stage is slow stage which occurs in 50 fm/c and excited raminant of is got equilibrated in this stage and the Intermidiate mass fragement (IMF A>4) and heavy fragment is emmited in this stage of reaction.

2.1 First stage reaction models

There are various first stage are available which is developed from many decades of the years.I will try to list and describe few of them.

2.1.1 Intranuclear cascade models - INC

The models which assume, that the interactions of high-energy particles with the nucleus can be represented by free particle-particle collisions inside the nucleus are called intranuclear cascade models. The 1st code of INC has

been created by Bertini . In 1963. Later, the conception was used also in other codes, e.g. by Yariv in his ISABEL code. In the 80's and 90's, the next versions of INC model was developed by Cugnon et al.(Now known as INCL++ or INCL 4.6). In this thesis only INCL was used for validation of different proton induced reaction. The INCL models are very similar to each other that why I will try to describe the INC models with the example of INCL model.

Target Nucleus

The spatial distribution of nucleons inside the target nucleus is prepared according to a Saxon-Woods formula

$$\rho = \begin{cases} \frac{\rho_0}{1+\exp(\frac{R-r_0}{a})} & R < R_{max} \\ 0 & R > R_{max} \end{cases} \tag{2.1}$$

where $R_{max} = r_{int} + R_0 + a$ and $r_{int} = (\sigma_{NN}^{tot}/\pi)^{\frac{1}{2}}$ R_0 and a are taken from electron scattering measurements and parametrized for Al to U as below

$$R_0 = (2.7545 * 10^{-4} A_T + 1.063) A_T^{1/3} \tag{2.2}$$

$$a = 0.510 + 1.63 * 10^{-4} A_T \tag{2.3}$$

The initial position and momentum of any target nucleon are generated as follows:is taken at random in a sphere of radius P_F
R(p) is calculated by relation

$$\left(\frac{P}{P_F}\right)^3 = -\frac{4\pi}{3A_T} \int_0^{R(p)} \frac{d\rho(r)}{dr} r^3 dr. \tag{2.4}$$

Potential

Isospin and energy-dependent potential well for the Nucleons Average potential for pions: An average isospin dependent Potential well of the Lane type is introduced for pions. Deflection of charged particles in the Coulomb field: Once an impact parameter is selected for the incident nucleon, the cascade process is initiated with this nucleon located at the intersection of the "external" Coulomb trajectory (corresponding asymptotically to the specific impact parameter) with the "working sphere". Nucleons move inside the

nucleus along straight trajectories until two of them collide or until one nucleon reaches the nucleus surface, where it can be transmitted or reflected. Division into participants and spectators.

Collisions between nucleons

The collision takes place when the distance between two nucleons is smaller than.

$$d \leq \sqrt{\sigma_{tot}/\pi} \tag{2.5}$$

where σ_{tot} is the total nucleon-nucleon cross section The following possible reactions are considered: $NN \rightarrow NN,\ NN \rightarrow N\Delta,\ N\Delta \rightarrow N\Delta,\ \Delta\Delta \rightarrow \Delta\Delta,\ \pi N \rightarrow \Delta$

Pauli Blocking

The quantum effectsare not totally neglected, i.e. the Pauli blocking is introduced for occupation of the final states which might be populated due to the collision. The light charged particles (LCP) can be emitted as result of Coalescence . the stopping time of the cascade is determined self-consistently by the model itself. It parametrized (in fm/c) by:

$$t_{stop} = 29.8 A_T^{0.16} \tag{2.6}$$

Cluster Emission

An outgoing nucleon arriving at the surface of the "working sphere," whether or not it has made collisions earlier, is selected as a possible leading nucleon for cluster emission, provided its energy is larger than the threshold energy, otherwise it is reflected. Potential clusters are then constructed. The leading nucleon is drawn on its (straight) line of motion back to a radial distance $D = R_0 + h$.

Chapter 3

Mechanisms of proton-nuclear target interaction – anisotropic production of pions and H isotopes

3.1 p+ Nb @ 3.5 GeV measured in HADES@GSI

3.2 Description of experiment

3.2.1 RICH

3.2.2 MDC

3.2.3 TOF/TOFino

3.3 Methodology of data analysis

3.3.1 issues in data analysis

3.3.2 Description of analysis

3.3.3 Establishing of systematic uncertainties

Chapter 4

Results for HADES data

Chapter 5

Mechanisms of isotropic emission of IMF and heavy target remnants

5.1 136Xe + p at 1GeV/A

5.2 comparison of total isotopic cross section with the models in broad range of Z and A

5.3 conclusions about the predictive power of the models and range of their usage

5.4 conclusion about the mechanisms used in individual models

Chapter 6

Further limitations of the models of IMF emission – the odd-even staggering in total production cross sections

To estimate experimentally the relative rate of non-equilibrium processes one has to know both, the total production cross section of given IMF and the cross section for its non-equilibrium emission. The total production cross section may be in principle obtained by a straightforward integration over energy and scattering angle of the experimental differential cross sections $d\sigma/d\Omega dE$, however the production cross section of given IMF due to a non-equilibrium process cannot be extracted from the experiment without additional model assumptions. The most promising method for this purpose seems to be substraction of the *equilibrium* emission cross section of given IMF from its total production cross section. Such a method should give value of the non-equilibrium production cross section as reliable as that of the equilibrium emission processes.

6.1 IMF production cross sections in p + Ag reaction at 480 MeV

It was demonstrated in the recent publications concerning predictive power of various reaction models used for the description of isotopic production cross

sections in p+^{136}Xe collisions at 1 GeV/nucleon [8] and at 0.5 GeV/nucleon [10] as well as for the analysis of differential cross sections of spallation reactions in p+Ag collisions at 0.48 GeV/nucleon [11] that the description of data by GEMINI model[12, 13][ref AIEEE] coupled to INCL4.6 [14] is superior in respect to those obtained with three other, popular models of the second stage of the reaction, namely ABLA07 [7], SMM [15] and GEM2 [16, 17]. Moreover, it was found that among the above listed models only GEMINI does not produce cross sections which exceed magnitude of the experimental data leaving a room for another reaction mechanism contributing incoherently to the reactions studied [11].

The following procedure has been used for the estimation of the equilibrium processes contribution to the production of the intermediate mass fragments. It was assumed that the collision of proton impinging on to the silver target proceeds as the two step process. The INCL++ model (version 5.3) [5] of the intranuclear cascade has been used for description of the first, fast stage of the collisions. A possibility of the emission of complex light charged particles in this stage of the process has been taken into account to assure achieving a realistic mass, charge and excitation energy distribution of the residual compound nuclei. However, the coalescence of the nucleons escaping from the intranuclear cascade with creation of intermediate mass fragments was not allowed because of two reasons: (i) the INCL++ enables one to perform efficiently such calculations only for the lightest IMF [14] and, (ii) it was found in the earlier study of these reactions [11] that high energy spectra of IMF are significantly overestimated by this model. It is important to emphasize that the above decision does not modify significantly the mass, charge and energy distribution of the excited nuclei - the remnants of the cascade since the cross sections for production of IMF are orders of magnitude smaller than those for nucleons and complex LCP. The second stage of the process, i.e., emission of particles from the excited compound nuclei - residuals of the fast stage of the reactions was described by GEMINI++ model [**GEMINI++**]. The results of the above calculations were treated as a realistic estimation for the total as well as for differential cross sections of equilibrated emission of IMF.

To obtain the total production cross section, the GEMINI++ double differential cross sections $d^2\sigma/dEd\Omega$ were supplied by incoherently added isotropic emission from highly excited Maxwellian source (or two sources) moving along the beam direction. The parameters of the source, i.e., its velocity β, apparent temperature T, the contribution to the total cross section

σ and the parameters responsible for the Coulomb barrier hindering the emission of ejectiles from the source were fitted to reproduce simultaneously the spectra of given ejectile at all scattering angles. Details of the moving source model as well as the interpretation of its parameters can be found in the Appendix of Ref.[18].

Very good reproduction of most of the data was achieved using one moving source contribution. This is illustrated by Fig. 6.1 in which experimental (dots) and model (lines) energy spectra of ^{18}O particles are depicted at three scattering angles: 20°, 90° and 160°. As can be seen, the equilibrium emission evaluated according to GEMINI++ [**GEMINI++**] coupled to INCL++ [5] model (solid, blue line) gives practically isotropic contribution whereas the non-equilibrium emission represented by single moving source (dashed, red line) dominates at forward scattering angle but it is much smaller than equilibrium cross sections at backward angles. The sum of both contributions (solid, black line) satisfactorily well reproduces the data.

Only 10 lightest IMF among all 39 studied particles, *i.e.*, ^{6,7}Li, ^{7,9,10}Be, ^{10,11,12}B and ^{11,12}C needed application of two moving sources for the good reproduction of energy spectra at all investigated scattering angles from 20° to 160°. An example of obtained quality of the data reproduction is presented in Fig. 6.2 where the energy spectra of ^{9}Be emitted at the same scattering angles as in Fig. 6.1, *i.e.*, 20°, 90° and 160° are shown. The equilibrium emission contribution represented by solid, blue line is in this case significantly smaller than the data for all scattering angles. For forward scattering angle and small energies the slower of both moving sources gives dominating contribution - shown as a dashed, red line - whereas the contribution of faster of the moving sources - depicted as a dotted, magenta line - reproduces the high energy tail of the spectrum. The situation is different for large scattering angle where the slower moving source dominates again for small energies but it gives comparable to the faster source contribution to the cross section at high energies. This is a typical situation for all analyzed spectra for which introduction of two moving sources was necessary.

The procedure described above enabled us to obtain non-equilibrium production cross section of IMF equal to the parameter σ_2 of the slow moving source (or to the sum of σ_2 and σ_3 - the appropriate parameters of both moving sources). Furthermore, sum of the equilibrium production cross section evaluated by means of GEMINI++ and the above non-equilibrium cross section provided value of the total production cross section.

The total cross sections due to INCL++ [5] coupled to GEMINI++

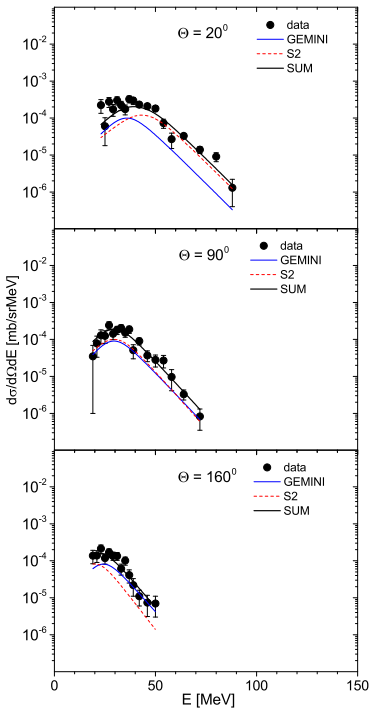

Figure 6.1: Experimental data (dots) and theoretical spectra for Ag(p,^{18}O) at three scattering angles: 20 degree (top panel), 90 degree (middle panel) and 120 degree (lower panel). The blue (solid) line represents GEMINI++ spectra, the red (dashed) line depicts contribution from additional moving source (S2), whereas the black (thick solid) line shows sum of both contributions.

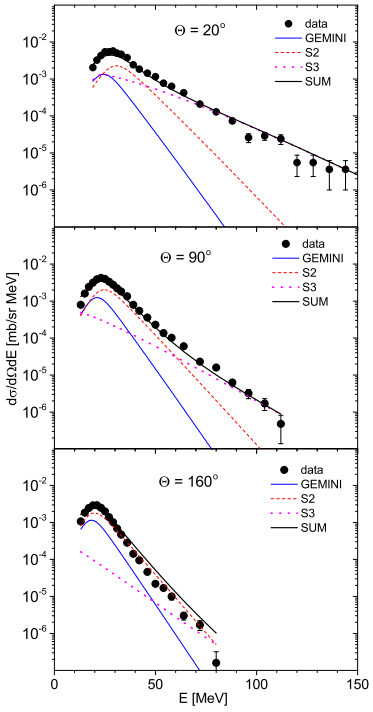

Figure 6.2: Experimental data (dots) and theoretical spectra for Ag(p,^{9}Be) at three scattering angles: 20 degree (top panel), 90 degree (middle panel) and 120 degree (lower panel). The blue (solid) line represents GEMINI++ spectra, the red (dashed) line depicts contribution from slower moving source (S2), the magenta (dotted) line shows contribution of the second, faster source (S3) whereas the black (thick solid) line shows sum of all contributions.

[**GEMINI++**] as well as the total cross sections obtained by fit of moving sources are presented together in Fig. 6.3 as a function of the atomic mass number of ejectiles. In the lower panel of the figure the equilibrium emission cross sections σ_{GEMINI} are shown, in the middle panel the non-equilibrium cross sections parameterized by slower of the moving sources σ_2 are depicted, whereas that due to the faster moving source σ_3 are shown in the upper panel of the figure. The cross sections for individual elements are presented by the same symbols and are connected by lines.

It is clear that the cross sections decrease in average as a function of the atomic mass number, however, this dependence of the cross sections is

non-monotonic, parabola - like for each individual element. It is important to note that the mass number A of the maximal cross section determined by the INCL+GEMINI model for given element is not always the same as the mass number A at which the maximal cross section of the non-equilibrium emission appears. Furthermore, variation of the equilibrium cross sections with the mass number seems to be more rapid than variation of the corresponding non-equilibrium cross sections. Therefore it is quite difficult to predict from this figure how complicated may be the mass dependence of the ratio of non-equilibrium cross sections to the total production cross sections $\sigma_{\rm NEQ}/\sigma_{\rm TOT}$, *i.e.*, to the sum of the equilibrium and non-equilibrium cross sections.

This quantity, which constitutes the subject of the present study is presented in Fig. 6.4 as a function of atomic mass number A of produced IMF. Different symbols connected by thin lines indicate values of the ratio for corresponding elements shown in the description at the right hand side of the figure. The same symbol depicts results obtained for various isotopes of a given element. The horizontal line placed at 0.5 value of the ratio divides the set of all isotopes into two groups; one with the ratio corresponding to the dominance of the equilibrium processes and the second of the opposite property.

The following properties of the ratio of the non-equilibrium cross sections to the total cross sections may be easily derived from this figure: (i) The ratios larger than 0.5 are about 2 times more abundant than those smaller than 0.5. This is true for both, small and large values of the atomic mass number A. (ii) Values of ratios close to 0.5 appear mainly at average mass number values (A $\sim$ 17) whereas those at smaller as well as at larger mass numbers are grouped into two separate sets. One set of the isotopes with the ratios smaller than 0.5 and the second set with the ratios larger than 0.5 for the same A values.

Such a specific dependence of the ratio $\sigma_{\rm NEQ}/\sigma_{\rm TOT}$ indicates that there exists no single monotonic trend of this ratio versus mass number A for all studied isotopes. One has to find some additional criterion which might select the isotopes into groups behaving in the same way when treated as a function of the mass number.

Two specific properties of the emitted intermediate mass fragments were applied for this purpose:

(i) the even/odd number of protons and neutrons - constituents of the IMF, and

(ii) the third component of the isospin of the fragment $\rm T_3 \equiv (N - Z)/2$

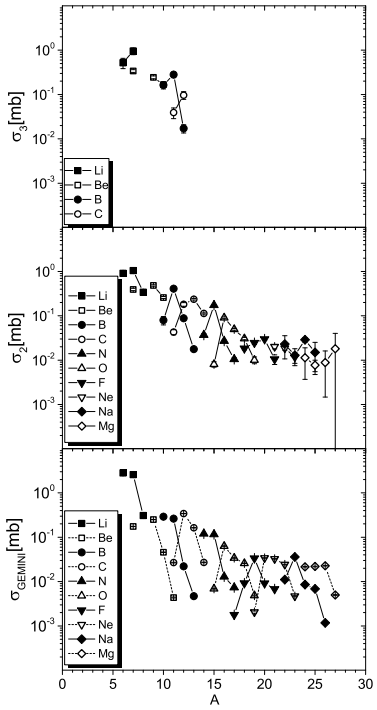

Figure 6.3: Production cross sections of intermediate mass fragments evaluated by means of the INCL++ model coupled to the GEMINI++ one (lower panel), production cross sections σ_2 from the phenomenological slow moving source (middle panel) and those (σ_3) due to the fast moving source (upper panel). Different elements are distinguished by using different symbols whereas various isotopes of the same element are represented by the same symbol.

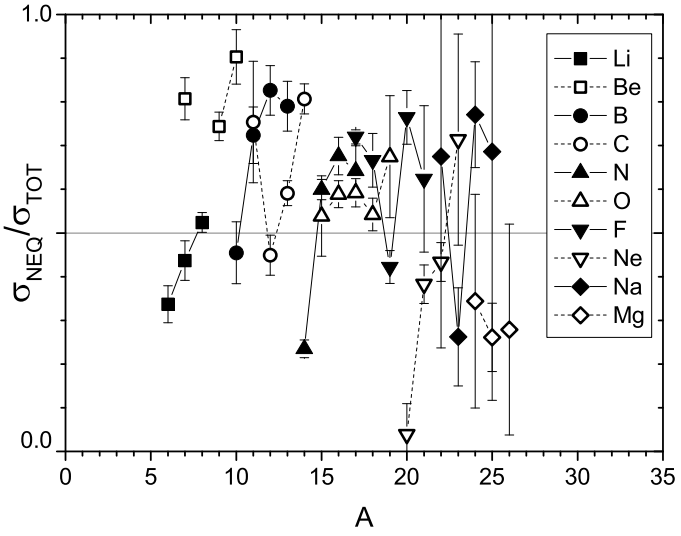

Figure 6.4: Atomic mass number A dependence of the ratio of non-equilibrium production cross section to the total production cross section for intermediate mass fragments emerging from p+Ag collisions.

representing excess (deficiency) of the number of neutrons in respect to the number of protons. For this purpose all reaction products were divided into 4 subgroups of definite (Z,N): (even - even), (even - odd), (odd - even) and (odd - odd). The atomic mass dependence of the ratio $\sigma_{\rm NEQ}/\sigma_{\rm TOT}$ was presented for these subgroups in separate panels of the Fig. 6.5; the upper-left panel for even-even (Z,N), the upper-right one for even-odd, *etc.*, in the clockwise direction.

It turned out that the ratio $\sigma_{\rm NEQ}/\sigma_{\rm TOT}$ behaves in a very regular way for each of these selected groups of isotopes (cf. Fig. 6.5). Especially, it may be stated that this ratio decreases in average linearly with the mass number A of emitted fragment for even-even, even-odd and odd-even intermediate mass fragments whereas it increases in average linearly for odd-odd ejectiles.

Furthermore, some deviations from such a regular behaviour may be observed for specific values of the third component of the isospin $T_3 \equiv (N-Z)/2$ of the emitted particles. For example, two of the four even-even ejectiles with $T_3 = 0$, namely ^{12}C and ^{20}Ne have much smaller ratio $\sigma_{\rm NEQ}/\sigma_{\rm TOT}$ than other even-even IMF with $T_3 = 0$ and all $T_3 = 1$ particles (cf. upper, left panel of Fig. 6.5).

Second of such deviations is the fact that all $T_3 = 3/2$ nuclides for even-odd and odd-even ejectiles have larger $\sigma_{\rm NEQ}/\sigma_{\rm TOT}$ ratio than that which characterizes the $T_3 = -1/2$ and $T_3 = 1/2$ nuclides (cf. upper-right and lower-right panel of the Fig. 6.5).

The third example consists in the systematic deviation toward smaller ratio values of $T_3 = 0$ ejectiles in respect to the straight line averaging behaviour of the odd-odd group of ejectiles whereas the IMF with $T_3 = 1$ deviate toward larger ratio values (cf. lower-left panel of the Fig. 6.5).

While no physical model has been implied by the dependence presented in the Fig. 6.5, the extremely regular behaviour achieved in this analysis certainly merits further consideration.

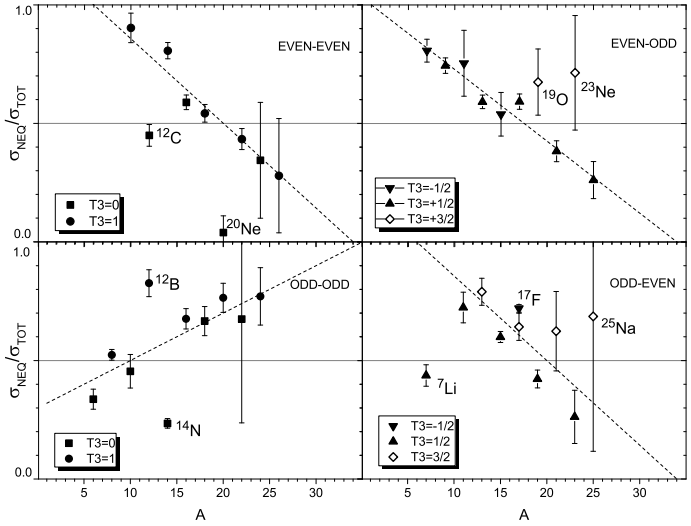

Figure 6.5: Atomic mass number A dependence of the ratio of non-equilibrium production cross section to the total production cross section for intermediate mass fragments emerging from p+Ag collisions. Left upper panel of the figure presents the results for even-even (Z,N) products whereas other panels (in clockwise direction) contain results for even-odd, odd-even and odd-odd products. Different symbols are attributed to values of the ratio corresponding to different values of the third component of the isospin $T_3 = (N - Z)/A$ of ejectiles. Dashed lines are drawn to guide the eye.

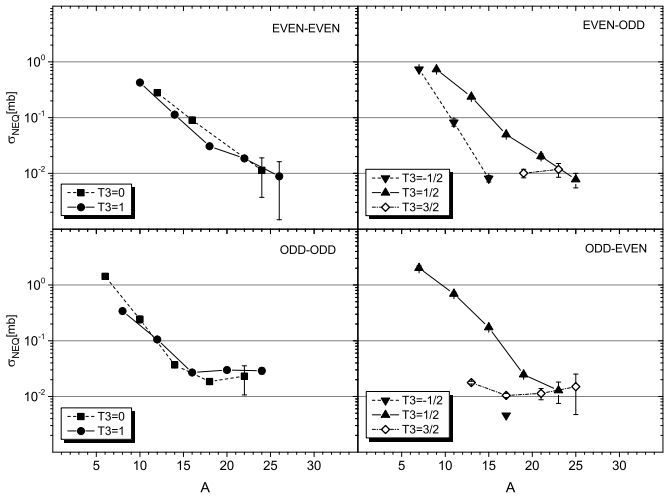

Figure 6.6: Atomic mass number dependence of the production cross sections of intermediate mass fragments emerging due to non-equilibrium processes from p+Ag collisions. Left upper panel of the figure presents the results for even-even (Z,N) products whereas other panels (in clockwise direction) contain results for even-odd, odd-even and odd-odd products. Different symbols are attributed to values of the cross sections for fragments with different values of the third component of the isospin $T_3 = (N - Z)/A$. The solid, dashed and dot-dashed lines are drawn to guide the eye.

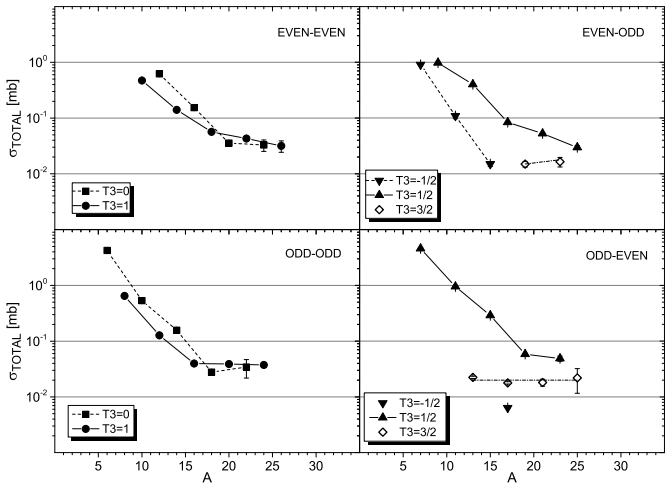

Figure 6.7: The same as in Fig. 6.6 but for the total production cross sections, *i.e.*, for the sum of equilibrium and non-equilibrium production cross sections. The solid, dashed and dot-dashed lines are drawn to guide the eye.

6.2 Hybrid (phenomenological+microscopic) approach to describe the double-differential cross sections features of total cross sections – odd-even staggering

6.3 Comparison of models and conclusion about their limitation

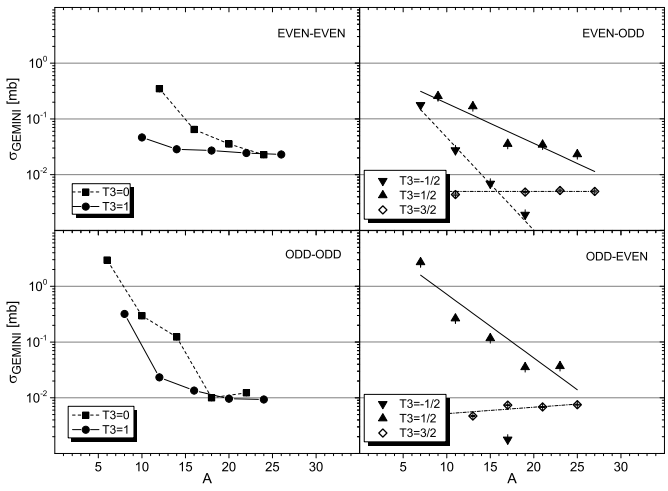

Figure 6.8: The same as in Fig. 6.6 but for the equilibrium emission cross sections evaluated by means of the INCL++ plus GEMINI++ models. The solid, dashed and dot-dashed lines are drawn to guide the eye.

Chapter 7

Dependence of non-equilibrium component in the production of IMF on the neutron number excess

7.1 Determination of non-equilibrium cross-section of IMF in p + Ag reaction at 480 MeV

7.2 Dependence of this component on third component of isospin

Chapter 8

Summary

8.1 Validation of total cross-section

The following analyzes were performed using the p+Ag and p+ 136 Xe data: Investigation of the quality of reproduction of the isotopic production cross sections for emission of different isotopes of the Li, Be, ... Ba nuclei from collisions of 1 GeV protons with 136 Xe by combination of two models: The INCL++ model describing fast, non-equilibrium phase of the collisions coupled to ABLA07,GEM,GEMINI and SMM models which were used to reproduce the second phase of the process, i.e. -emission of products from equilibrated remnant of the first stage of the processes.(This is the content of published paper [8])

8.2 Validation of differential cross-section for IMF and heavy products

Analysis of angular distributions for double differential cross sections $d\sigma/d\Omega dE$ for intermediate mass fragments (isotopes of Li, Be, ... Mg elements) emitted from p+Ag reaction at E p =0.48 GeV with the aim to extract:

- Contribution of the non-equilibrium processes to the reaction,
- Dependence of the isotopic total cross sections of these reactions on the izospin degree of freedom.

(This is the content of [UNPUB] paper prepared for publication in EPJA but rejected by referees) Investigation of the odd-even staggering in the yields of IMFs from the above reac- tion, i.e. p+Ag collisions at E p =0.48 GeV with the aim to study a possibility to validate models of the spallation reactions using this degree of freedom. (This is the content of Acta Phy)

8.3 LCP data analysis and validation of different models

Determination of differential cross sections $d\sigma/d\Omega dE$ for emission of Hydrogen isotopes as well as pions (π^+ and π^-) using raw data stored event-by-event from collisions of protons with Nb nuclei at E p =3.5 GeV in HADES collaboration experiment performed at GSI in Sep 2008. Theoretical analysis of these data by means of following theoretical models like INCL++ ,BUU, UrQMD, JAM. The above investigations of HADES data were performed with the aim to shed light on the first, non-equilibrium part of the proton-nucleus collisions whereas the analysis of the literature data for p+Ag and p+ 136 Xe gave a chance to obtain information on the mechanism of the second, slow stage of the collision process which appears after equilibration of the excited remnant of the target nucleus.

Bibliography

[1] J. M. Carpenter, Nuclear Instruments and Methods **145**, 91 (1977).

[2] H. Ravn, Philosophical Transactions of the Royal Society A: Mathematical, Physical and Engineering Sciences **356**, 1955 (1998).

[3] C. Bowman, E. Arthur, P. Lisowski, G. Lawrence, R. Jensen, J. Anderson, B. Blind, M. Cappiello, J. Davidson, T. England, L. Engel, R. Haight, H. Hughes, J. Ireland, R. Krakowski, R. LaBauve, B. Letellier, R. Perry, G. Russell, K. Staudhammer, G. Versamis, and W. Wilson, Nuclear Instruments and Methods in Physics Research Section A: Accelerators, Spectrometers, Detectors and Associated Equipment **320**, 336 (1992).

[4] M. Meneguzzi, J. Audouze, and H. Reeves, Astronomy and Astrophysics **15**, 337 (1971).

[5] D. Mancusi, A. Boudard, J. Cugnon, J.-C. David, P. Kaitaniemi, and S. Leray, Phys. Rev. C **90**, 054602 (2014).

[6] A. Boudard, J. Cugnon, S. Leray, and C. Volant, Phys. Rev. C **66**, 044615 (2002).

[7] A. Kelic, M. V. Ricciardi, and K.-H. Schmidt, arXiv preprint arXiv:0906.4193 (2009).

[8] U. Singh, D. Filges, F. Goldenbaum, B. Kamys, Z. Rudy, and S. K. Sharma, The European Physical Journal A **54**, 1 (2018).

[9] U. Singh, B. Kamys, S. Sharma, and K. Pysz, Acta Physica Polonica. B **50**, 1451 (2019).

[10] S. K. Sharma, B. Kamys, F. Goldenbaum, and D. Filges, The European Physical Journal A **53**, 1 (2017).

[11] S. K. Sharma, B. Kamys, F. Goldenbaum, and D. Filges, The European Physical Journal A **52**, 1 (2016).

[12] R. Charity, M. McMahan, G. Wozniak, R. McDonald, L. Moretto, D. Sarantites, L. Sobotka, G. Guarino, A. Pantaleo, L. Fiore, A. Gobbi, and K. Hildenbrand, Nuclear Physics A **483**, 371 (1988).

[13] R. J. Charity, Phys. Rev. C **82**, 014610 (2010).

[14] A. Boudard, J. Cugnon, J.-C. David, S. Leray, and D. Mancusi, Physical Review C **87**, 014606 (2013).

[15] J. Bondorf, A. Botvina, A. Iljinov, I. Mishustin, and K. Sneppen, Physics Reports **257**, 133 (1995).

[16] S. Furihata, Nuclear Instruments and Methods in Physics Research Section B: Beam Interactions with Materials and Atoms **171**, 251 (2000).

[17] S. Furihata and T. Nakamura, Journal of Nuclear Science and Technology **39**, 758 (2002).

[18] A. Bubak, A. Budzanowski, D. Filges, F. Goldenbaum, A. Heczko, H. Hodde, L. Jarczyk, B. Kamys, M. Kistryn, A. Kowalczyk, et al., Physical Review C **76**, 014618 (2007).